Check for updates

Received: 18 April 2023 | Revised: 12 October 2023 | Accepted: 16 December 2023

DOI: 10.1002/ep.14340

ENVIRONMENTAL PROGRESS & SUSTAINABLE ENERGY

ORIGINAL RESEARCH

Sustainable Energy

# Green synthesis capacitor of carbon quantum dots from *Stachys euadenia*

Canan Baslak[1] | Serkan Demirel[2] | Suleyman Dogu[3] | Gulsah Ozturk[4] | Adem Kocyigit[5] | Murat Yıldırım[4]

[1]Department of Chemistry, Science Faculty, Selcuk University, Konya, Turkey

[2]Vocational High School, Department of Electric and Energy, Igdir University, Igdir, Turkey

[3]Meram Vocational School, Necmettin Erbakan University, Konya, Turkey

[4]Department of Biotechnology, Science Faculty, Selcuk University, Konya, Turkey

[5]Vocational High School, Department of Electronic and Automation, Bilecik Seyh Edebali University, Bilecik, Turkey

**Correspondence**
Adem Kocyigit, Vocational High School, Department of Electronic and Automation, Bilecik Seyh Edebali University, Bilecik, Turkey.
Email: adem.kocyigit@bilecik.edu.tr

## Abstract

Carbon quantum dots (CQDs) are a new type of carbon nanomaterial that has recently attracted great attention as a potential competitor to standard semiconductor quantum dots. There are various ways to synthesis CQDs, and one of harmless way is undoubtedly green synthesis. In this study, hydrothermal synthesis based on the green way was employed to synthesize CQDs. The CQDs were obtained using the green leaves of the *Stachys euadenia* plant extract, an endemic species located in Turkey. The CQDs were characterized by fluorescent and UV-Visible spectroscopy, and results confirmed blue emission (430–480 nm) and absorption around 280 nm. X-ray photoelectron spectroscopy (XPS) analysis revealed C=C, C–N and C–O interactions. X-ray diffractometer (XRD) patterns confirmed structure of carbon with a broad peak of (002) plane. High resolution tunneling electron microscopy (HRTEM) and dynamic light scattering (DLS) analysis was used to determine the shape and size of CQDs. The CQDs obtained from *Stachys euadenia* were employed as electrode materials for capacitor application, and they were tested in Swagelok-type cell by cyclic voltammetry (CV) measurements. CQD capacitors exhibited 2.12 F/g charge and 1.24 F/g discharge capacitances were obtained with ~58% coulombic efficiency rate for the first cycle. Results highlights that CQDs are synthesized successfully by green synthesis method and can be used for capacitor applications.

**KEYWORDS**
carbon quantum dots, green synthesis, *Stachys euadenia*, supercapacitor

## 1 | INTRODUCTION

Carbon quantum dots (CQDs) have received significant and increasing attention in both science and technology environment after their discovery at about two decades ago for various applications.[1–4] The increase in studies in this field depends on the unique physical properties and fluorescence (radiation) of carbon dots.[5,6] CQDs are nano-sized particles of carbon as an environmentally friendly alternative to toxic QDs, which have attracted great interest since 2006. It is known that fluorescent semiconductor quantum dots will lead to a wide variety of promising applications, especially in biology,[7] electronic[8,9] and medicine.[10–13] CQDs have many advantages due to their nontoxicity, photostability, high quantum yield, low cost, availability and high surface passivation. Other known properties of CQDs are their high biocompatibility, chemical inertness and high specific surface area.[14,15] CQDs synthesized harmless method, which are also produced from organic precursors, are particularly interesting for photo-electric applications.[16,17] Janus et al. investigated the preparation of smart, surface-modified CQDs with a bottom-up synthesis approach using bioproducts. In their work, they used a stainless-steel autoclave for hydrothermal synthesis.[18] The CQDs obtained at the end of the study were characterized by tunable fluorescence and up to 14% quantum

 © 2024 American Institute of Chemical Engineers. 

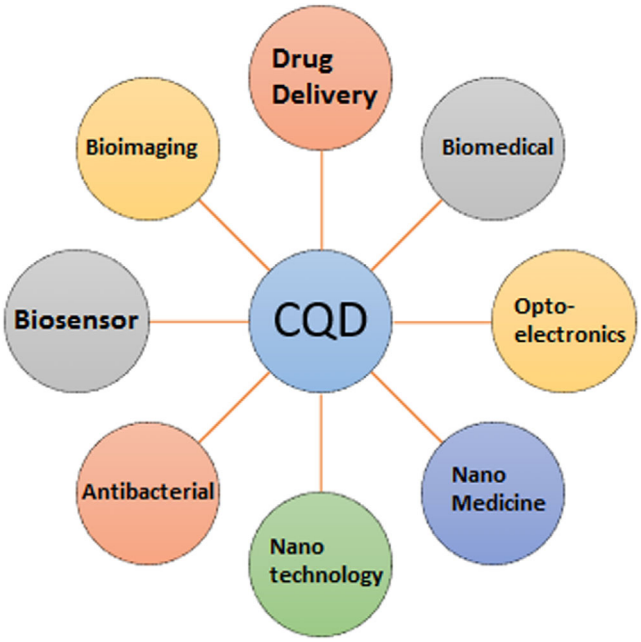


**FIGURE 1** Some application areas of CQDs.

efficiency. Molaei discussed the drug delivery system with CQDs in his research.[19] Thanks to many of the above-mentioned features of CQDs, they have good potential application in drug delivery systems. Various application areas of CQDs are listed in Figure 1 such as in nanofibers,[20,21] optoelectronics[22] and antibacterial applications.[23]

The photoluminescence properties of QDs are most relevant in the framework of chemical analysis. In the preparation of CQDs, three issues should be considered briefly: (i) chemical synthesis, (ii) uniformity, and (iii) surface properties. For plant-derived CQDs, the particle size is usually less than 10 nm. Hydrothermal synthesis, known as the chemical reaction method in aqueous solution, takes place under conditions of temperature of 100°C ~ 1000°C and pressure of 1 MPa ~ 1 GPa. The ions are mixed evenly in the aqueous solution, so the product has high purity, good dispersion and easy particle size control, and this is the most important advantage of hydrothermal synthesis.[24] There are many types of synthesizing biocompatible nanoparticles, one of these alternative ways is the green synthesis approach. The best eco-friendly alternative method is the plant extract-based synthetic approach compared to other biological methods and existing conventional physical as well as chemical methods.[25] In the hydrothermal synthesis method, substances are crystallized from an aqueous solution under high pressure using various techniques. The synthesis is carried out in a pressurized stainless-steel autoclave.[26] A solvent other than water cannot be used with the hydrothermal method. One of the most preferred methods in the production of carbon materials is the hydrothermal method. It has been the most preferred method in terms of environmental friendliness, low cost and convenience.[27–31]

Supercapacitors that store electrical charge at an electrode–electrolyte interface, primarily an electrical double layer on an electrode with a high surface area, are also known as electrochemical capacitors or ultracapacitors. These devices are known to provide high specific and volumetric energy and power dense activity with an unlimited charge–discharge cycle life due to the high surface area and small thickness of the double layer.[32] Coming to the forefront as energy storage devices, electrochemical supercapacitors have unique, superior properties such as high-power density and significantly long cycle life.[33] A supercapacitor basically consists of two electrodes, an electrolyte and a separator that electrically isolates two electrodes. The most important component in a supercapacitor is the electrode material.[34] Among the materials considered as possible electrode materials for industrialization are those of carbon origin. It has been determined that carbon materials, high specific surface area, increase the ability to accumulate charge at the electrode and electrolyte interface.[33]

The main aim of the study is to synthesize CQDs from *Stachys euadenia* in a short time using an environmentally friendly production technique with green approach synthesis, and to test their capacitor properties as electrode materials. Thus, we synthesized CQDs using a well-known and accepted hydrothermal method, which is a one-step, cheap and simple technique generally used for nano materials synthesis. The obtained CQDs have emitting strong and green fluorescence property. The CQDs electrode materials exhibited capacitive behavior in a Swagelok-type cell.

## 2 | EXPERIMENTAL

### 2.1 | Procuring *Stachys euadenia*

*Stachys euadenia* is a locally endemic plant species belonging to the *Lamiaceae* family. The *Stachys euadenia* we used in the experiment had green leaves. This little-known plant was introduced to the scientific world by P.H. Davis in 1951. It naturally spreads on lime rocks in Kazancı (Karaman) and Abanoz Plateau (Mersin) regions in Turkey between 1300- and 1850-m height. *Stachys euadenia* was picked up from Kazancı region for synthesizing CQDs.

### 2.2 | Method

#### 2.2.1 | Solution preparation

Dry *Stachys euadenia* leaves were ground with a grinder. 0.5 g was weighed from the grinded leave and taken into 60 mL of pure water. It was made homogeneous mixing in a 400-rpm magnetic stirrer at 60°C for 1 h. One milliliter of ethylenediamine was added to the homogeneous solution.

#### 2.2.2 | Hydrothermal synthesis

The solution was taken into the stainless-steel autoclave. The oven was set 150°C for 4 h. Autoclave was placed in the oven reaching 150°C. After 24 h, the autoclave taken from the oven was opened.

19447450, 2024, 3, Downloaded from https://aiche.onlinelibrary.wiley.com/doi/10.1002/ep.14340 by Bilecik Seyh Edebali, Wiley Online Library on [05/12/2025]. See the Terms and Conditions (https://onlinelibrary.wiley.com/terms-and-conditions) on Wiley Online Library for rules of use; OA articles are governed by the applicable Creative Commons License


**FIGURE 2** Synthesis of CQDs obtained from *Stachys euadenia*.

### 2.2.3 | CQD purification

A coarse centrifugation was applied to the sample for 3 min at 4000 rpm. Then, ultracentrifuge was applied to the separated liquid sample at 15,000 rpm for 10 min. In order to make it purer and finer, large particles were removed by ultracentrifugation, and filtered by a syringe filter. The purified sample was dried in a glass petri dish at room temperature for 48 h. The production scheme of the whole study is shown in Figure 2.

## 2.3 | Characterization of CQDs

Synthesized CQDs from *Stachys euadenia* was characterized by fluorescence spectroscopy, UV-Vis spectroscopy, XRD, HRTEM, XPS and DLS instruments. The spectrometric properties of CQDs fluorescence spectra were measured on a LS 55 fluorescence spectrophotometer. The ultraviolet-visible (UV-Vis) absorption spectrum was measured using a UV-1280 (Shimadzu) spectrophotometer. A JEOL JEM 2100 HRTEM brand high-resolution tunneling electron microscopy was used for imaging of CQDs. X-ray diffraction patterns of CQDs were recorded with a Bruker Advance D8 XRD (Cu a source with 1.5406 Å wavelength) in powder mode. To determine the oxidation levels of metals, organic, inorganic, polymers, physical and chemical properties of materials; X-ray photoelectron spectroscopy analysis was performed with a Thermo-K-Alpha X-ray Photoelectron Spectroscopy equipped with a monochromatic Al/Kα as the X-ray source. DLS analysis was performed with a MALVERN/ DLS MPT2 instrument to measure the intensity and variation of light scattered from small particles in dilute solution of CQDs.

## 2.4 | Electrochemical tests

The electrochemical tests were utilized with Gamry brand 1010-E model potentiostat system. The symmetric capacitors were built with Swagelok-type cell. The CQDs were used as electrode material (symmetrically) and 6 mol KOH (aq) solution was used as an electrolyte. A cellulosic paper membrane was used as a separator. Cyclic voltammetry (CV) measurements were utilized for determination the reaction kinetics and energy storage properties. The CV measurements were carried out at a constant scan speed of 200, 400, 800, and 1200 mV/s. The cycle life study capacitance measurements were performed under 200 mV/s constant scanning speed in a range of 0–1.7 V. Afterwards, the capacitance values of the samples were calculated as like in the reference.[35]

# 3 | RESULTS AND DISCUSSION

## 3.1 | Characterization results of CQDs

The fluorescence emission and absorption spectrums of the CQDs have been illustrated in Figure 3a,b, respectively. CQDs exhibited the most intense emission when excited at 380 nm. According to the fluorescence emissions spectrum, the emission intensity is

19447450, 2024, 3, Downloaded from https://aiche.onlinelibrary.wiley.com/doi/10.1002/ep.14340 by Bilecik Seyh Edebali, Wiley Online Library on [05/12/2025]. See the Terms and Conditions (https://onlinelibrary.wiley.com/terms-and-conditions) on Wiley Online Library for rules of use; OA articles are governed by the applicable Creative Commons License

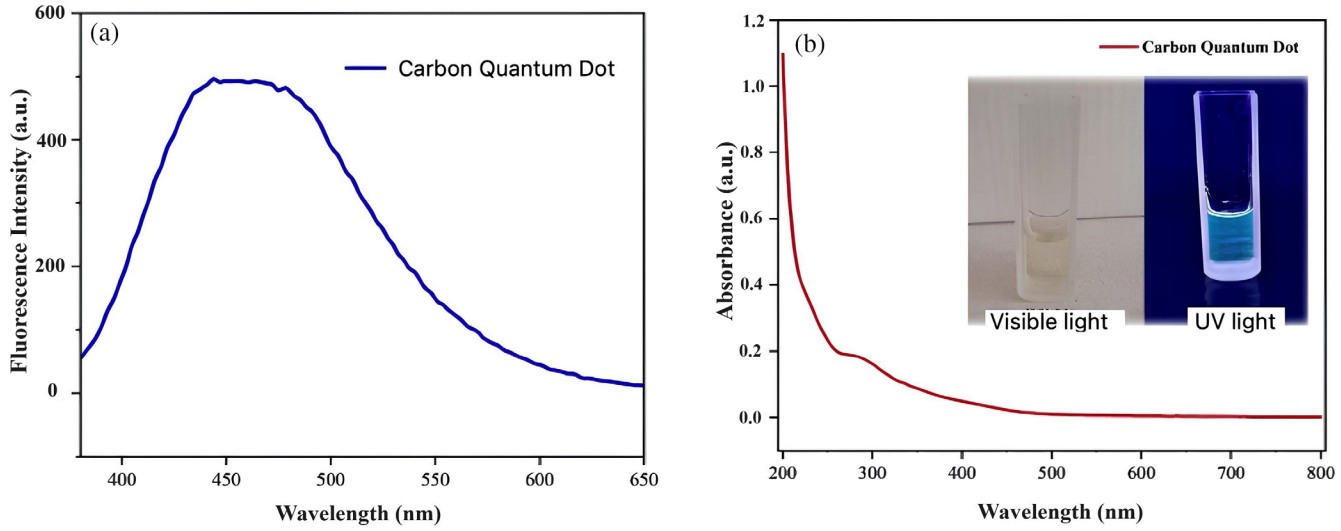


**FIGURE 3** (a) Fluorescence and (b) absorption spectra of CQDs.

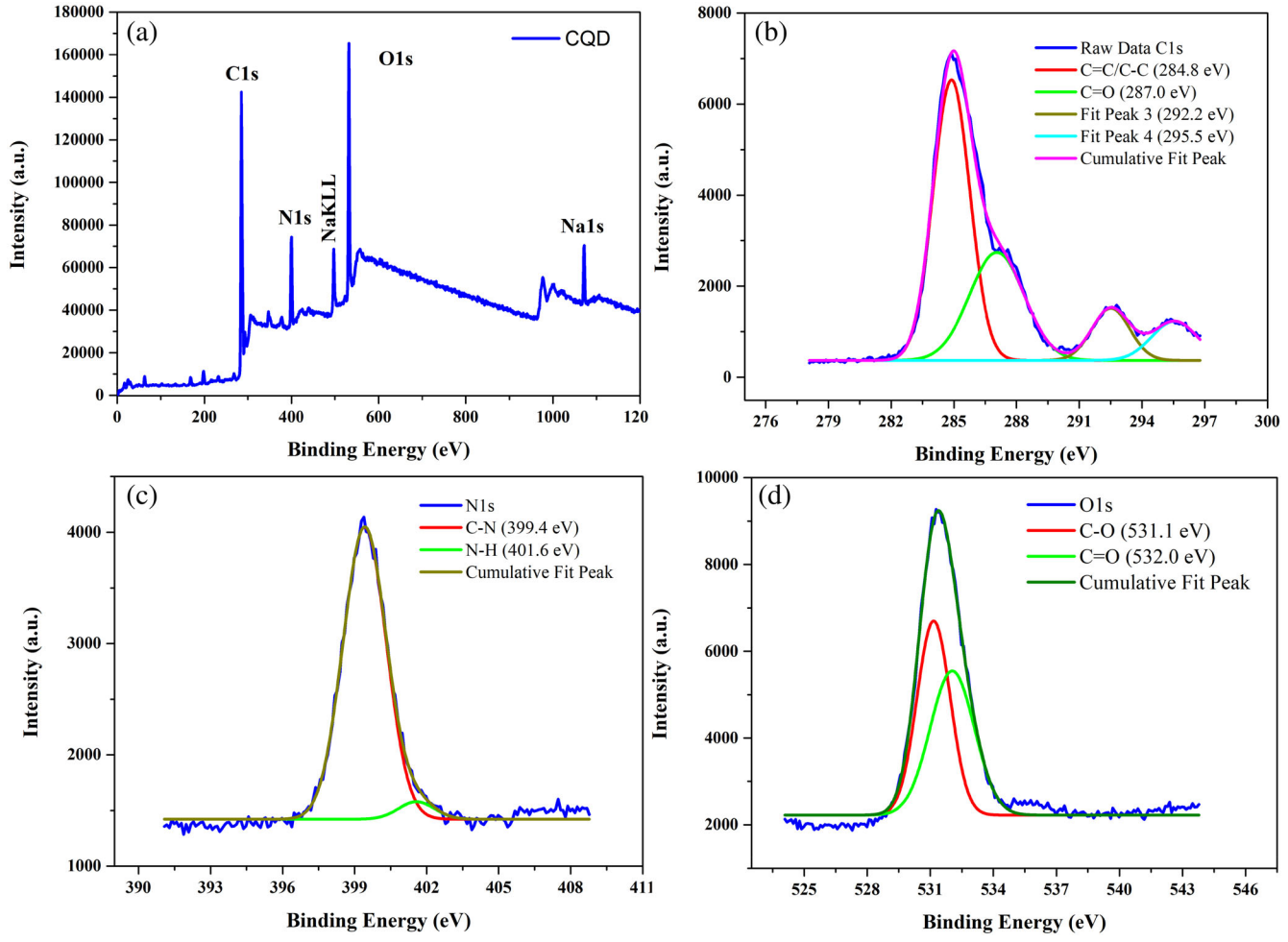


**FIGURE 4** X-ray photoelectron spectroscopy of CQDs: (a) wide scan XPS survey, (b) C1s spectrum, (c) N1s spectrum, and (d) O1s spectrum of the CQDs.

19447450, 2024, 3, Downloaded from https://aiche.onlinelibrary.wiley.com/doi/10.1002/ep.14340 by Bilecik Seyh Edebali, Wiley Online Library on [05/12/2025]. See the Terms and Conditions (https://onlinelibrary.wiley.com/terms-and-conditions) on Wiley Online Library for rules of use; OA articles are governed by the applicable Creative Commons License

maximum in the range of 430–480 nm. According to the inset image in Figure 3a, it can be seen that CQDs emit blue radiation under the UV lamp while their solution is white under visible light. Figure 3b indicates the absorption spectra of the CQDs, and an absorption has been seen at 280 nm wavelength. This peak is the characteristic absorption peak of CQDs and is attributed to the $\pi$–$\pi^*$ transition. This florescence emission and absorption spectrum were obtained for CQDs by various plants in the literature.[36–38]

XPS analysis was performed to obtain chemical information about the functional groups and chemical structure present on the surface of the synthesized CQDs. Figure 4a–d shows the XPS analysis results. While Figure 4a has showed the wide scan XPS survey, Figure 4b–d shows the C1s spectrum, N1s spectrum, and O1s spectrum of the CQDs, respectively. As shown in Figure 4a, the wide scan XPS survey of CQDs from *Stachys euadenia* revealed three intense peaks. The first peak represents C1s, the second one represents the N1s, and the third peak is for O1s. There is a pollution in transport water that occurs 440 eV. According to the results of the analysis as shown in Figure 4b, the peaks at 284.8 eV and 287.0 can be attributed to C=C/C–C, C=O interactions. The peaks at 399.4 eV and 401.6 eV seen in Figure 4c refer to C–N and N–H bonding. The relevant Figure 4d for the O1 spectrum gives two dominated peaks at 531.1 eV and 532.0 eV, and these are attributed to C–O and C=O bonding. From the high-resolution XPS scan results, we have confirmed that mainly C and N are present in the CQDs structures.[39–41]

XRD patterns of CQDs are provided in Figure 5a. Characteristic peak for CQDs is clearly observed on the XRD patterns. The respective XRD patterns of CQDs show a single broad diffraction peak at $2\theta = 22.15^\circ$ for the (002) plane. The value obtained for CQDs is consistent with the values in the literature, which are in the range of 20–25°.[42–44] HRTEM measurements were used to view the morphological structures of the CQDs. Figure 5b indicate HRTEM image as well as DLS results. The obtained CQDs have an almost similar size distribution and their diameter distribution range is around 18–20 nm. Furthermore, the particles are quasispherical with essentially amorphous core structure and without a crystal lattice. They appear to be slightly flattened from the sides and have a vague gap in the middle. DLS analysis was performed to determine the particle size distribution of synthesized CQDs. The inset of Figure 5b exhibits the DLS results of the CQDs synthesized from *Stachys euadenia* plant. According to the results of the analysis, DLS measurements also have confirmed the TEM images, and the particle size distribution of CQDs is 20 nm on average.[45–48]

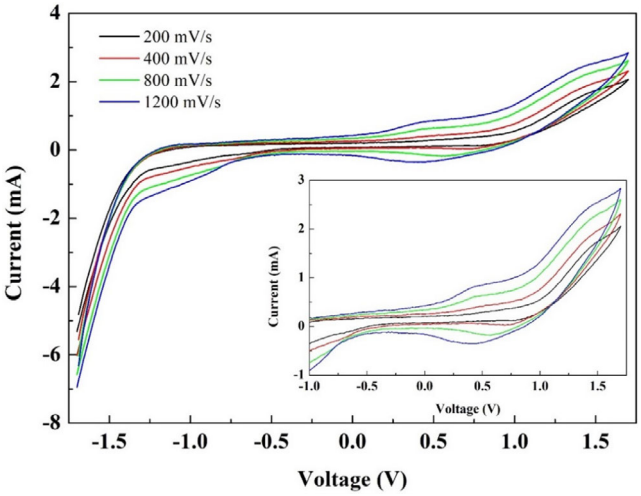


**FIGURE 6** Electrochemical characterization via cyclic voltammogram.

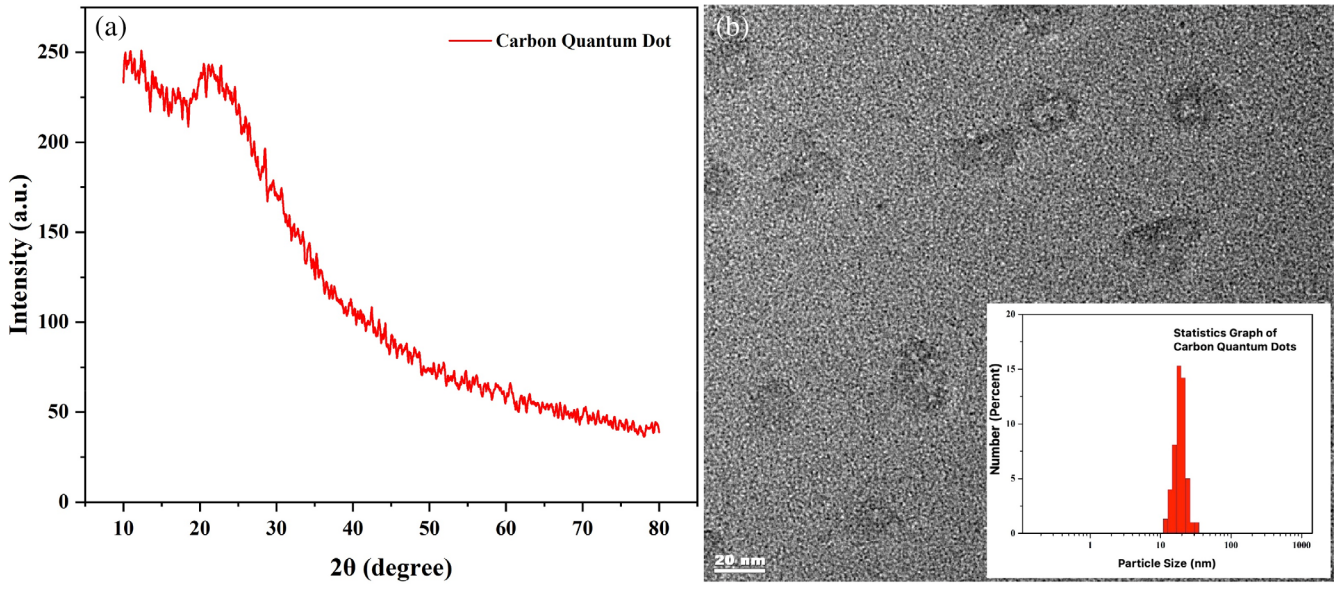


**FIGURE 5** (a) XRD pattern and (b) TEM image and particle size distribution histogram of the CQDs from DLS.

19447450, 2024, 3, Downloaded from https://aiche.onlinelibrary.wiley.com/doi/10.1002/ep.14340 by Bilecik Seyh Edebali, Wiley Online Library on [05/12/2025]. See the Terms and Conditions (https://onlinelibrary.wiley.com/terms-and-conditions) on Wiley Online Library for rules of use; OA articles are governed by the applicable Creative Commons License

### 3.2 | Electrochemical characterization

The electrochemical analyses for CQDs were initiated by CV measurements. The voltage–current characteristics of the CQDs have been seen in Figure 6. It has been observed that some faradaic reactions may occur, especially in the cathodic current region (0–1.70 V and positive current region). Two different reactions were observed in the cathodic region while a single reaction formation was observed in the anodic region. Due to the that high CV scanning rates and broad peak formations may affect the reaction kinetic analysis wrongly, dI/dV analysis should be performed to determine the voltage ranges of these reactions and the changes.

Figure 7a,b shows the dI/dV analysis of CQDs electrode capacitors for cathodic and anodic regions, respectively. While the capacitive current behavior is observed at 200 and 400 mV/s scanning rates between 0.10 and 0.50 V, a new oxidation peak occurs in this region at 800 and 1200 mV/s scanning rates according to Figure 7a. The oxidation peaks were determined at 0.38 V and 0.30 V levels for 800 and 1200 mV/s scanning rates, respectively. These redox peaks, which appeared due to the increasing scanning speed, revealed the pseudocapacitive electrode feature of CQDs.[49] Similarly, the pseudocapacitive electrode feature was observed with redox peaks occurring in the 1.20–1.30 V range at all scanning speeds and all scanning speeds. Figure 7b exhibits the dI/dV analysis for the determination of reduction reactions for the anodic region. In the first look for *Stachys euadenia* CQDs, which generally exhibit capacitive current behavior in the anodic region, and it may be wrong to talk about the presence of a redox reaction in this region. However, in the inset graph seen in Figure 6, it was observed that the broad peaks formed at ~1 V (at 200 mV/s) decreased to 0.43 V (at 1200 mV/s) with increasing scanning speed. This behavior in the anodic region is generally thought to be caused by the electrode-electrolyte interface. A detailed study of the electrode–electrolyte interactions is in progress for a more precise reaction description. Based on these results, it has been determined that *Stachys euadenia* CQDs exhibited clearly cathodic characteristics.

Figure 8 displays the initial charge–discharge analysis of the symmetric CQD capacitors. In particular, the fact that CQDs performed two oxidation reactions in the cathodic region, and these reactions were not reversible showed a direct effect on the charge and discharge capacitance values. 2.12 F/g charge and 1.24 F/g discharge capacitances were obtained with ~58% coulombic efficiency rate for the first cycle. While the effect of the double faradaic reaction is seen to be effective on the charge capacitance, the nonreversibility of these reactions causes the lower discharge performance. In particular, the inhibition of Faradaic reactions is thought to be due to the fact that *Stachys euadenia* CQDs electrodes do not allow electrolyte ion diffusion. The fact that the diffusion of $K^+$ and $OH^-$ ions to the electrodes is not at desired levels, and that Faradaic reactions are not reversible are effective in the decrease of capacitive performance.[50] Of course, as the most important factors in this situation is production of symmetrical capacitors, and the use of K-based KOH electrolyte according to Li and Na elements as electrolyte active material can be

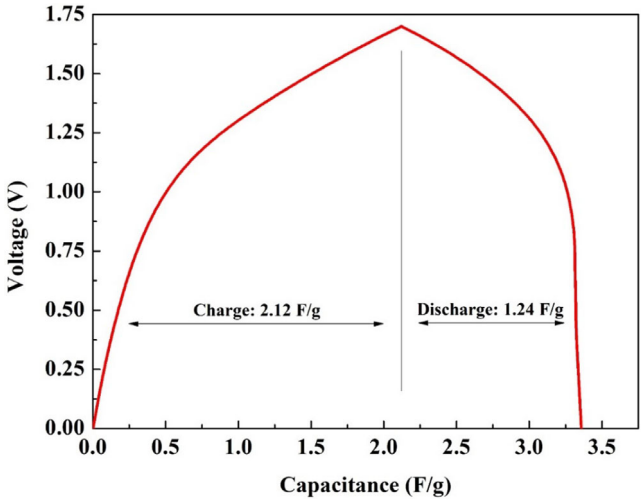


**FIGURE 8** The first charge–discharge capacitive performance with Faradaic reactions effectiveness.

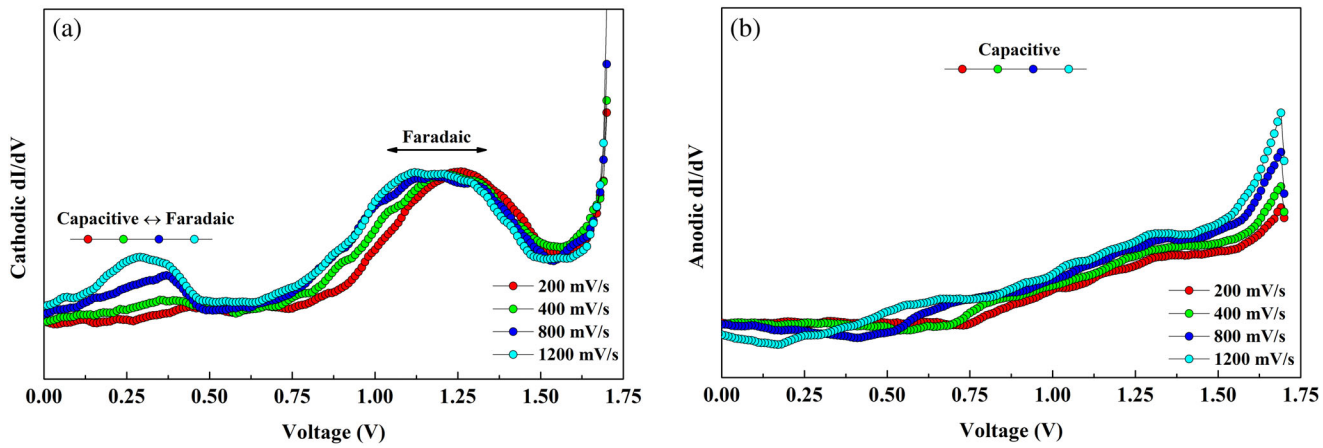


**FIGURE 7** Redox reaction analysis via dI/dV calculation: (a) the cathodic region and (b) the anodic region.

19447450, 2024, 3, Downloaded from https://aiche.onlinelibrary.wiley.com/doi/10.1002/ep.14340 by Bilecik Seyh Edebali, Wiley Online Library on [05/12/2025]. See the Terms and Conditions (https://onlinelibrary.wiley.com/terms-and-conditions) on Wiley Online Library for rules of use; OA articles are governed by the applicable Creative Commons License

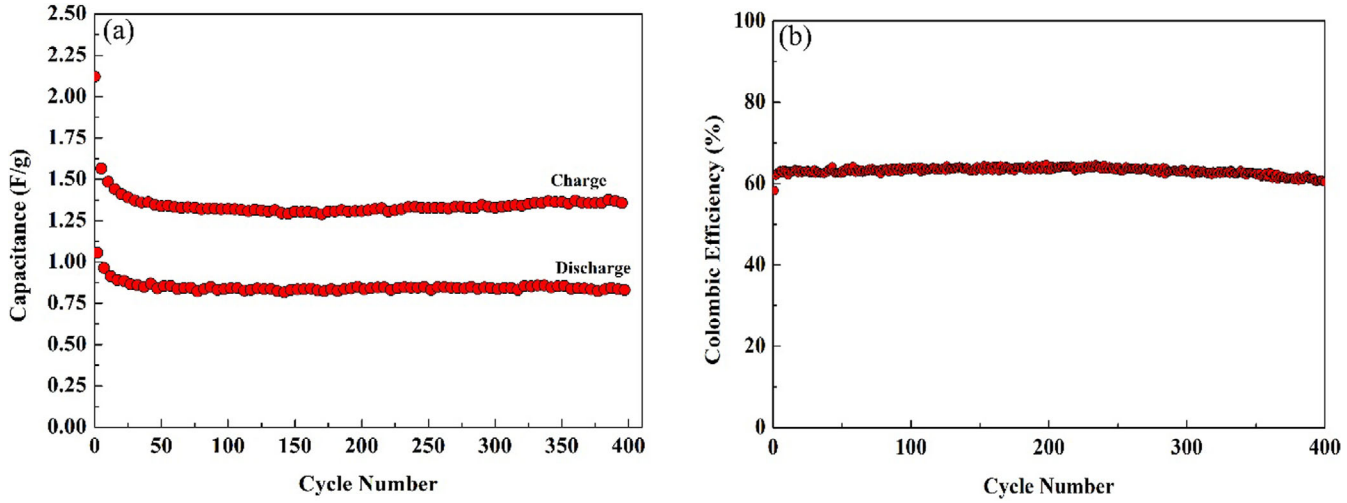


**FIGURE 9** Capacitive performance analysis during 400 cycles. (a) Cycle life performance and (b) the coulombic efficiency.

**TABLE 1** CR values of the CQD symmetric capacitor.

| | 1st cycle | 100th cycle | 200th cycle | 400th cycle | CR (%) |
|---|---|---|---|---|---|
| Charge | 2.12 | 1.32 | 1.31 | 1.36 | 35.8 |
| Discharge | 1.24 | 0.84 | 0.83 | 0.83 | 33.1 |

shown as a reason. Pillai et al. showed that higher capacitive performance could be obtained with LiOH and NaOH in their study with LiOH, NaOH and KOH, in 2015.[51]

Figure 9 shows the charge–discharge performance of CQD capacitors for 400 cycles. According to Figure 9a, the discharge performance started with 1.24 F/g, decreased during the first 20 cycles and dropped of 0.84 F/g levels. However, this decrease was interrupted after 20 cycles, and the capacitor exhibited a stable discharge performance in between 0.84–0.87 F/g capacitance values. A similar decrease was observed for charging performance. The initial charge capacitance value of 2.12 F/g decreased to 1.34 F/g at the end of the 20 cycles. The charge capacitance obtained an average of 1.34 F/g during 250 cycles reached an average of 1.36 F/g end of 250 cycles. Based on these obtained values, capacity retention (CR) has been calculated with Equation 1, and their values are given in Figure 9b and Table 1.

$$CR = \frac{C_0 - C_n}{C_0} \times 100 \quad (1)$$

where $C_0$ is the first cycle capacitance value, and $C_n$ is the last cycle capacitance value.

The coulombic efficiency values were calculated as 58% according to the first charge–discharge cycle, and this reached 63% after the second cycle. The capacitor exhibited a coulombic efficiency performance of 63% for approximately 250 cycles, and decreased to 60% in the last 150 cycles. This decrease, especially after 250 cycles, is clearly seen in Figure 9a. After an average of 250 cycles, an increase of 0.04 F/g occurred in the charge capacitance values. However, it

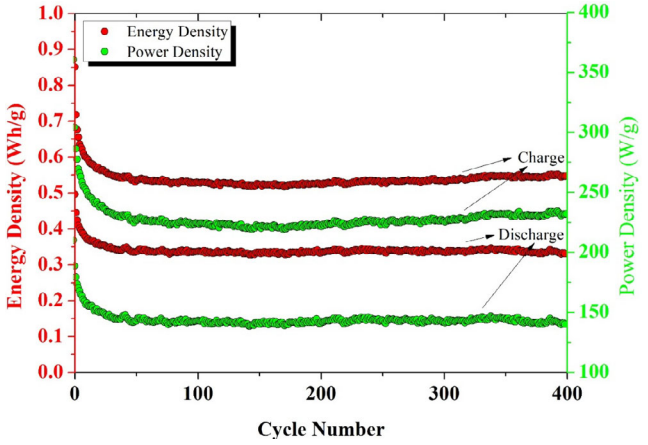


**FIGURE 10** Energy and power density comparison of CQD capacitors.

has been determined that this positive performance improvement in the charging mechanism is not reflected to the discharge performance. The *Stachys euadenia* CQDs exhibited stable anodic performance over 400 cycles. Therefore, a small decrease in the coulombic efficiency rate was observed. It is known that under normal conditions, coulombic efficiency values of high-performance batteries and capacitors exhibit values of 90% and above.[52–54] However, *Stachys euadenia* CQD capacitors offer an average of 62% coulombic efficiency and have a medium capacitive performance with this value.

According to the calculated CR values in Table 1, 34%–35% retention occurs specifically in the range of 1–400 cycles. Generally, measurements of 1000–10,000 cycles are made in experimental

19447450, 2024, 3, Downloaded from https://aiche.onlinelibrary.wiley.com/doi/10.1002/ep.14340 by Bilecik Seyh Edebali, Wiley Online Library on [05/12/2025]. See the Terms and Conditions (https://onlinelibrary.wiley.com/terms-and-conditions) on Wiley Online Library for rules of use; OA articles are governed by the applicable Creative Commons License

**TABLE 2** Energy and power density amounts for some specific cycles.

| | 1st cycle | | 100th cycle | | 200th cycle | | 400th cycle | |
|---|---|---|---|---|---|---|---|---|
| | *E* (Wh/g) | *P* (W/g) | *E* (Wh/g) | *P* (W/g) | *E* (Wh/g) | *P* (W/g) | *E* (Wh/g) | *P* (W/g) |
| Charge | 0.85 | 360.53 | 0.53 | 224.37 | 0.52 | 222.31 | 0.55 | 232.10 |
| Discharge | 0.49 | 210.17 | 0.34 | 142.74 | 0.33 | 140.93 | 0.33 | 140.15 |

capacitor studies, and when the results obtained in general are examined, it has been determined that the values obtained after an average of 100 cycles are stable in the range of 1000–10,000 cycles.[55,56] However, when the obtained values are examined, it can be said that the average CQDs symmetrical capacitors can exhibit stable performance after an average of 50 cycles.

The energy (*E*) and power (*P*) densities were also calculated depending on charge and discharge capacitance values by following Equations (2) and (3), and the values showed as a graph in Figure 10[57]:

$$E = \frac{1}{2} C \Delta V^2 \tag{2}$$

$$P = \frac{E}{t} \times 3600 \tag{3}$$

where *C* is the capacitance (F/g), $\Delta V$ is the potential window, and *t* is the time. When the energy and power density amounts are calculated from the capacitance values, the energy density of 0.85 Wh/g and a power density of 360.53 W/g are charged for the first cycle. In case of discharge, 0.49 Wh/g energy density and 210.17 W/g power density are provided.

The energy and power density amounts of CQD capacitors for various cycles have been listed in Table 2. According to Table 2, CQD capacitors provide stable energy and power density after an average of 50 cycles. At the end of 400 cycles, the energy density of 0.55 Wh/g, and a power density of 232.10 W/g are obtained for charging process. In case of discharge, 0.33 Wh/g energy density and 140.15 W/g power density are provided. Obtaining such low power and energy density values based on capacitive performance for supercapacitors shows that *Stachys euadenia* CQDs electrodes cannot be operated very successfully with KOH electrolyte. However, it has been discovered that *Stachys euadenia* CQDs electrodes have a supercapacitive effect compared to normal capacitors, with a discharge performance of approximately 1.00 F/g.

Among the supercapacitor applications electric double-layered capacitor (EDLC), asymmetric capacitor (AC), hybrid capacitor (HC), CQD-based capacitors have a relatively newer history, and usually it is seen that CQDs have a very important effect for EDLC applications.[58] In addition, in modifications made with metal oxides such as $MnO_2$, $Fe_2O_3$, $Co_3O_4$, etc., CQDs also provide significant increases in capacitor performance (capacitance, cycle-life stability, etc.).[59–61] The main reasons for these performance increase in CQDs electrodes are increasing the electrical conductivity of the electrode, creating a high surface area, and contributing to polarization by interacting with redox-active electrolytes.[62,63] Especially the polarization effect creates an important performance contribution for EDLC capacitors. Despite the high capacitance and performance-enhancing contributions of CQDs electrodes, the low capacitance values obtained in our study are thought to be due to the application of symmetrical capacitors.[63] This situation provides a disadvantage in terms of polarization effect compared to AC, HC, and EDLC types.

## 4 | CONCLUSION

The CQDs were synthesized successfully and easily by green synthesis hydrothermal method from green leaves of the *Stachys euadenia* plant extract, an endemic plant of Turkey. The CQDs were characterized by fluorescent spectroscopy, UV-Visible spectroscopy, XPS, XRD, HRTEM and DLS instruments. While the fluorescent spectroscopy results showed blue emission in the wavelength range of 430–480 nm, the UV-Visible spectrum exhibited absorption around 280 nm. XPS analysis revealed C=C, C–N, and C–O interactions for 284.8 eV, 399.4 eV, and 531.1 eV binding energies, respectively. XRD pattern exhibit (002) characteristics broad carbon peak around 20–25°. HRTEM and DLS analysis revealed that shape and size of CQDs were almost quasi-spherical and 18–20 nm. The electrochemical analyses of the CQDs as electrode materials for capacitor indicated that the electrodes of CQDs had 2.12 F/g charge capacitance and 1.24 F/g discharge capacitance obtained with ~58% coulombic efficiency rate for the first cycle. Results highlighted that CQDs were can be improved for capacitor applications.

### AUTHOR CONTRIBUTIONS

**Adem Kocyigit:** Writing – review and editing; supervision. **Canan Baslak:** Methodology; writing – original draft; visualization. **Serkan Demirel:** Writing – original draft; data curation; visualization. **Suleyman Dogu:** Methodology. **Gulsah Ozturk:** Data curation. **Murat Yıldırım:** Data curation; writing – review and editing; supervision.

### FUNDING INFORMATION

The authors declare that no funds, grants, or other support were received during the preparation of this manuscript.

### CONFLICT OF INTEREST STATEMENT

The authors declare that they have no known competing financial interests or personal relationships that could have appeared to influence the work reported in this paper.

19447450, 2024, 3, Downloaded from https://aiche.onlinelibrary.wiley.com/doi/10.1002/ep.14340 by Bilecik Seyh Edebali, Wiley Online Library on [05/12/2025]. See the Terms and Conditions (https://onlinelibrary.wiley.com/terms-and-conditions) on Wiley Online Library for rules of use; OA articles are governed by the applicable Creative Commons License

## DATA AVAILABILITY STATEMENT

Data are available on request from the authors.

## STATEMENT OF INDUSTRIAL RELEVANCE

There is no industrial relevance of the paper.

## NOVELTY STATEMENT

This paper contains green synthesis of the carbon quantum dots from *Stachys euadenia* plant and its supercapacitor application for a long-term stability.

## ORCID

*Adem Kocyigit* https://orcid.org/0000-0002-8502-2860

## REFERENCES


1. Xu X, Ray R, Gu Y, et al. Electrophoretic analysis and purification of fluorescent single-walled carbon nanotube fragments. *J Am Chem Soc*. 2004;126(40):12736-12737. doi:10.1021/ja040082h
2. Dong D, Liu T, Liang D, et al. Facile hydrothermal synthesis of chlorella-derived environmentally friendly fluorescent carbon dots for differentiation of living and dead chlorella. *ACS Appl Bio Mater*. 2021;4(4):3697-3705. doi:10.1021/acsabm.1c00178
3. Wu C, Zheng Y, Wang W, Liu Y, Yu J, Liu Y. Phase behavior and aggregate transition based on Co-assembly of negatively charged carbon dots and a pH-responsive tertiary amine cationic surfactant. *Langmuir*. 2022;38(45):13771-13781. doi:10.1021/acs.langmuir.2c01895
4. Liu X, Liu W, Zuo K, Zheng J, Wang M, Liu X. High color stability blue-to-violet room temperature phosphorescent carbon dot composites with UItralong lifetime for information encryption. *ACS Sustain Chem Eng*. 2023;11(5):1809-1819. doi:10.1021/acssuschemeng.2c06094
5. Jelinek R. Synthesis, Properties and Applicatons. *Carbon quantum dots*. *Springer International Publishing*; 2017:29-46.
6. Jing H, Bardakci F, Akgöl S, et al. Green carbon dots: synthesis, characterization, properties and biomedical applications. *J Funct Biomater*. 2023;14(1):27. doi:10.3390/jfb14010027
7. Jamieson T, Bakhshi R, Petrova D, Pocock R, Imani M, Seifalian AM. Biological applications of quantum dots. *Biomaterials*. 2007;28(31):4717-4732. doi:10.1016/j.biomaterials.2007.07.014
8. Zhang J, Jin J, Wan J, et al. Quantum dots-based hydrogels for sensing applications. *Chem Eng J*. 2021;408:127351. doi:10.1016/j.cej.2020.127351
9. Bozal-Palabiyik B, Kurbanoglu S, Erkmen C, Uslu B. Future prospects and concluding remarks for electroanalytical applications of quantum dots. *Electroanalytical Applications of Quantum Dot-Based Biosensors*. Elsevier; 2021:427-450. doi:10.1016/B978-0-12-821670-5.00008-7
10. Sun Y-P, Zhou B, Lin Y, et al. Quantum-sized carbon dots for bright and colorful photoluminescence. *J Am Chem Soc*. 2006;128(24):7756-7757. doi:10.1021/ja062677d
11. Gaur M, Misra C, Yadav AB, et al. Biomedical applications of carbon nanomaterials: fullerenes, quantum dots, nanotubes, nanofibers, and graphene. *Materials (Basel)*. 2021;14(20):5978. doi:10.3390/ma14205978
12. Hamed AA, Saad GR, Abdelhamid IA, Elwahy AHM, Abdel-Aziz MM, Elsabee MZ. Chitosan Schiff bases-based polyelectrolyte complexes with graphene quantum dots and their prospective biomedical applications. *Int J Biol Macromol*. 2022;208:1029-1045. doi:10.1016/j.ijbiomac.2022.03.199
13. Ren Q, Ma Y, Zhang S, Ga L, Ai J. One-step synthesis of water-soluble silver sulfide quantum dots and their application to bioimaging. *ACS Omega*. 2021;6(9):6361-6367. doi:10.1021/acsomega.0c06276
14. Pinilla-Peñalver E, García-Béjar B, Contento AM, Ríos Á. Graphene quantum dots an efficient nanomaterial for enhancing the photostability of trans-resveratrol in food samples. *Food Chem*. 2022;386:132766. doi:10.1016/j.foodchem.2022.132766
15. Sun J, Du H, Chen Z, Wang L, Shen G. MXene quantum dot within natural 3D watermelon peel matrix for biocompatible flexible sensing platform. *Nano Res*. 2022;15(4):3653-3659. doi:10.1007/s12274-021-3967-x
16. Al-mebir AAK, AL-Saidi SAA. Tuning optoelectronic properties of double quantum dot structure using tight-binding model for photoelectric applications. *NeuroQuantology*. 2021;19(3):1-10. doi:10.14704/nq.2021.19.3.NQ21021
17. Maria Semeniuk MS, Yi Z, Poursorkhabi V, Tjong J, Jaffer S, Zheng-Hong L. Future perspectives and review on organic carbon dots in electronic applications. *ACS nano*. 2019;13(6):6224-6255. doi:10.1021/acsnano.9b00688
18. Janus Ł, Radwan-Pragłowska J, Piątkowski M, Bogdał D. Facile synthesis of surface-modified carbon. *Materials*. 2020;13(15):3313.
19. Molaei MJ. Principles, mechanisms, and application of carbon quantum dots in sensors: a review. *Anal Methods*. 2020;12(10):1266-1287. doi:10.1039/C9AY02696G
20. Nie X, Wu S, Mensah A, Lu K, Wei Q. Carbon quantum dots embedded electrospun nanofibers for efficient antibacterial photodynamic inactivation. *Mater Sci Eng C*. 2020;108:110377. doi:10.1016/j.msec.2019.110377
21. Saud PS, Pant B, Alam A-M, Ghouri ZK, Park M, Kim H-Y. Carbon quantum dots anchored TiO2 nanofibers: effective photocatalyst for waste water treatment. *Ceram Int*. 2015;41(9):11953-11959. doi:10.1016/j.ceramint.2015.06.007
22. Zhang Z, Zheng T, Li X, Xu J, Zeng H. Progress of carbon quantum dots in Photocatalysis applications. *Part Part Syst Charact*. 2016;33(8):457-472. doi:10.1002/ppsc.201500243
23. Subashini K, Prakash S, Sujatha V. Polymer nanocomposite prepared using copper oxide nanoparticles derived from Sterculia foetida leaf extract with biological applications. *Mater Res Express*. 2020;7(11):115308. doi:10.1088/2053-1591/abc979
24. Lou Y, Hao X, Liao L, et al. Recent advances of biomass carbon dots on syntheses, characterization, luminescence mechanism, and sensing applications. *Nano Sel*. 2021;2(6):1117-1145. doi:10.1002/nano.202000232
25. Yuvakkumar R, Suresh J, Nathanael AJ, Sundrarajan M, Hong SI. Novel green synthetic strategy to prepare ZnO nanocrystals using rambutan (*Nephelium lappaceum* L.) peel extract and its antibacterial applications. *Mater Sci Eng C*. 2014;41:17-27. doi:10.1016/j.msec.2014.04.025
26. Byrappa K, Yoshimura M, Yoshimura M. *Handbook of Hydrothermal Technology*. William Andrew; 2001.
27. Krishnaiah P, Atchudan R, Perumal S, Salama E-S, Lee YR, Jeon B-H. Utilization of waste biomass of Poa pratensis for green synthesis of n-doped carbon dots and its application in detection of Mn2+ and Fe3+. *Chemosphere*. 2022;286:131764. doi:10.1016/j.chemosphere.2021.131764
28. Atchudan R, Edison TNJI, Perumal S, Muthuchamy N, Lee YR. Hydrophilic nitrogen-doped carbon dots from biowaste using dwarf banana peel for environmental and biological applications. *Fuel*. 2020;275:117821. doi:10.1016/j.fuel.2020.117821
29. Atchudan R, Edison TNJI, Perumal S, Vinodh R, Lee YR. Betel-derived nitrogen-doped multicolor carbon dots for environmental and biological applications. *J Mol Liq*. 2019;296:111817. doi:10.1016/j.molliq.2019.111817
30. Atchudan R, Edison TNJI, Aseer KR, Perumal S, Karthik N, Lee YR. Highly fluorescent nitrogen-doped carbon dots derived from Phyllanthus acidus utilized as a fluorescent probe for label-free selective detection of Fe3+ ions, live cell imaging and fluorescent ink. *Biosens Bioelectron*. 2018;99:303-311. doi:10.1016/j.bios.2017.07.076


19447450, 2024, 3, Downloaded from https://aiche.onlinelibrary.wiley.com/doi/10.1002/ep.14340 by Bilecik Seyh Edebali, Wiley Online Library on [05/12/2025]. See the Terms and Conditions (https://onlinelibrary.wiley.com/terms-and-conditions) on Wiley Online Library for rules of use; OA articles are governed by the applicable Creative Commons License

31. Atchudan R, Edison TNJI, Chakradhar D, Perumal S, Shim J-J, Lee YR. Facile green synthesis of nitrogen-doped carbon dots using Chionanthus retusus fruit extract and investigation of their suitability for metal ion sensing and biological applications. *Sens Actuators B*. 2017;246:497-509. doi:10.1016/j.snb.2017.02.119
32. Avinash Balakrishnan KRVS. *Nanostructured Ceramic Oxides for Supercapacitor Applications*. CRC Press; 2014. doi:10.1201/b16522
33. Scibioh MA, Viswanathan B. *Materials for Supercapacitor Applications*. Elsevier; 2020. doi:10.1016/c2019-0-00454-2
34. Iro ZS, Subramani C, Dash SS. A brief review on electrode materials for Supercapacitor. *Int J Electrochem Sci*. 2016;11:10628-10643. doi:10.20964/2016.12.50
35. Demirel S. Bloedite-type Na2X(SO4)2 (X = Ni, Mg) as novel alternative aqueous electrolyte materials for supercapacitors. *J Mater Sci Mater Electron*. 2020;31(22):19809-19818. doi:10.1007/s10854-020-04505-1
36. Boruah A, Saikia M, Das T, Goswamee RL, Saikia BK. Blue-emitting fluorescent carbon quantum dots from waste biomass sources and their application in fluoride ion detection in water. *J Photochem Photobiol B Biol*. 2020;209:111940. doi:10.1016/j.jphotobiol.2020.111940
37. Jiang S, Chen Y, Duan G, Mei C, Greiner A, Agarwal S. Electrospun nanofiber reinforced composites: a review. *Polym Chem*. 2018;9(20):2685-2720. doi:10.1039/C8PY00378E
38. Wu Y, Qin D, Meng S, Zhang C, Deng B. Carbon quantum dots with blue/near infrared emissions for ratiometric fluorescent lornoxicam sensing and bio-imaging. *Microchim Acta*. 2022;189(4):157. doi:10.1007/s00604-022-05262-0
39. Shereema RM, Sankar V, Raghu K, Rao TP, Shankar SS. One step green synthesis of carbon quantum dots and its application towards the Bioelectroanalytical and Biolabeling studies. *Electrochim Acta*. 2015;182:588-595. doi:10.1016/j.electacta.2015.09.145
40. Siahcheshm P, Heiden P. High quantum yield carbon quantum dots as selective fluorescent turn-off probes for dual detection of Fe2+/-Fe3+ ions. *J Photochem Photobiol A Chem*. 2023;435:114284. doi:10.1016/j.jphotochem.2022.114284
41. Guerrero-Gonzalez R, Vázquez-Dávila F, Saucedo-Flores E, Ruelas R, Ceballos-Sánchez O, Pelayo JE. Green approach synthesis of carbon quantum dots from agave bagasse and their use to boost seed germination and plant growth. *SN Appl Sci*. 2023;5(8):204. doi:10.1007/s42452-023-05428-2
42. Shaikh AF, Tamboli MS, Patil RH, Bhan A, Ambekar JD, Kale BB. Bioinspired carbon quantum dots: An Antibiofilm agents. *J Nanosci Nanotechnol*. 2018;19(4):2339-2345. doi:10.1166/jnn.2019.16537
43. Bajpai SK, D'Souza A, Suhail B. Blue light-emitting carbon dots (CDs) from a milk protein and their interaction with Spinacia oleracea leaf cells. *Int Nano Lett*. 2019;9(3):203-212. doi:10.1007/s40089-019-0271-9
44. Jaison AMC, Vasudevan D, Ponmudi K, George A, Varghese A. One pot hydrothermal synthesis and application of bright-yellow-emissive carbon quantum dots in Hg2+ detection. *J Fluoresc*. 2023;33:2281-2294. doi:10.1007/s10895-023-03233-z
45. de Oliveira EGL, de Oliveira HP, Gomes ASL. Metal nanoparticles/carbon dots nanocomposites for SERS devices: trends and perspectives. *SN Appl Sci*. 2020;2(9):1491. doi:10.1007/s42452-020-03306-9
46. Siddique AB, Pramanick AK, Chatterjee S, Ray M. Amorphous carbon dots and their remarkable ability to detect 2,4,6-Trinitrophenol. *Sci Rep*. 2018;8(1):9770. doi:10.1038/s41598-018-28021-9
47. Le HC, Pham NT, Vu DC, et al. Nitrogen-doped graphene quantum dot–tin dioxide nanocomposite ultrathin films as efficient electron transport layers for planar perovskite solar cells. *Crystals*. 2023;13(6):961. doi:10.3390/cryst13060961
48. Liu ML, Yang L, Li RS, Bin Chen B, Liu H, Huang CZ. Large-scale simultaneous synthesis of highly photoluminescent green amorphous carbon nanodots and yellow crystalline graphene quantum dots at room temperature. *Green Chem*. 2017;19(15):3611-3617. doi:10.1039/C7GC01236E
49. Zhai T, Wan L, Sun S, et al. Phosphate ion functionalized Co 3 O 4 ultrathin Nanosheets with greatly improved surface reactivity for high performance Pseudocapacitors. *Adv Mater*. 2017;29(7):1604167. doi:10.1002/adma.201604167
50. Chen T, Dai L. Carbon nanomaterials for high-performance supercapacitors. *Mater Today*. 2013;16(7–8):272-280. doi:10.1016/j.mattod.2013.07.002
51. Pillai AS, Rajagopalan R, Amruthalakshmi A, et al. Mesoscopic architectures of Co(OH) 2 spheres with an extended array of microporous threads as pseudocapacitor electrode materials. *Colloids Surf*. 2015;470:280-289. doi:10.1016/j.colsurfa.2015.01.068
52. Laheäär A, Przygocki P, Abbas Q, Béguin F. Appropriate methods for evaluating the efficiency and capacitive behavior of different types of supercapacitors. *Electrochem Commun*. 2015;60:21-25. doi:10.1016/j.elecom.2015.07.022
53. Sarkar S, Akshaya R, Ghosh S. Nitrogen doped graphene/CuCr2O4 nanocomposites for supercapacitors application: effect of nitrogen doping on coulombic efficiency. *Electrochim Acta*. 2020;332:135368. doi:10.1016/j.electacta.2019.135368
54. Krishnan SG, Reddy MV, Harilal M, et al. Characterization of MgCo2O4 as an electrode for high performance supercapacitors. *Electrochim Acta*. 2015;161:312-321. doi:10.1016/j.electacta.2015.02.081
55. Wu G, Tan P, Wang D, et al. High-performance Supercapacitors based on electrochemical-induced vertical-aligned carbon nanotubes and polyaniline nanocomposite electrodes. *Sci Rep*. 2017;7(1):43676. doi:10.1038/srep43676
56. Wang M, Peng A, Xu H, et al. Amorphous SnSe quantum dots anchoring on graphene as high performance anodes for battery/capacitor sodium ion storage. *J Power Sources*. 2020;469:228414. doi:10.1016/j.jpowsour.2020.228414
57. Huang C, Lv S, Gao A, et al. Boosting the energy density of supercapacitors by designing both hollow NiO nanoparticles/nitrogen-doped carbon cathode and nitrogen-doped carbon anode from the same precursor. *Chem Eng J*. 2022;431:134083. doi:10.1016/j.cej.2021.134083
58. Xiao J, Momen R, Liu C. Application of carbon quantum dots in supercapacitors: a mini review. *Electrochem Commun*. 2021;132:107143. doi:10.1016/j.elecom.2021.107143
59. Lv H, Gao X, Xu Q, Liu H, Wang Y-G, Xia Y. Carbon quantum dot-induced MnO 2 nanowire formation and construction of a binder-free flexible membrane with excellent Superhydrophilicity and enhanced Supercapacitor performance. *ACS Appl Mater Interfaces*. 2017;9(46):40394-40403. doi:10.1021/acsami.7b14761
60. Wei G, Zhao X, du K, et al. Flexible asymmetric supercapacitors made of 3D porous hierarchical CuCo2O4@CQDs and Fe2O3@CQDs with enhanced performance. *Electrochim Acta*. 2018;283:248-259. doi:10.1016/j.electacta.2018.06.153
61. Naushad M, Ahamad T, Ubaidullah M, et al. Nitrogen-doped carbon quantum dots (N-CQDs)/Co3O4 nanocomposite for high performance supercapacitor. *J King Saud Univ Sci*. 2021;33(1):101252. doi:10.1016/j.jksus.2020.101252
62. Wang C, Strauss V, Kaner RB. Carbon Nanodots for Capacitor Electrodes. *Trends Chem*. 2019;1(9):858-868. doi:10.1016/j.trechm.2019.05.009
63. Cherusseri J, Pandey D, Thomas J. Symmetric, asymmetric, and battery-type Supercapacitors using two-dimensional nanomaterials and composites. *Batter Supercaps*. 2020;3(9):860-875. doi:10.1002/batt.201900230

**How to cite this article:** Baslak C, Demirel S, Dogu S, Ozturk G, Kocyigit A, Yıldırım M. Green synthesis capacitor of carbon quantum dots from *Stachys euadenia*. *Environ Prog Sustainable Energy*. 2024;43(3):e14340. doi:10.1002/ep.14340

19447450, 2024, 3, Downloaded from https://aiche.onlinelibrary.wiley.com/doi/10.1002/ep.14340 by Bilecik Seyh Edebali, Wiley Online Library on [05/12/2025]. See the Terms and Conditions (https://onlinelibrary.wiley.com/terms-and-conditions) on Wiley Online Library for rules of use; OA articles are governed by the applicable Creative Commons License